Characteristics of urban vehicular MIMO channels at different frequencies

Tricia J. Willink
Communications Research Centre,
3701 Carling Ave., Ottawa, ON, K2H 8S2, CANADA
email: tricia.willink@crc.ca

***Abstract*—MIMO channel measurements at different UHF frequencies have been made in an urban vehicular environment. The data show that the spatial diversity decreases with frequency, attributed to an increase in scattering near the mobile receiver, resulting in weaker angular multipath components. The spatial structure of the channel changes more slowly, however, at lower frequencies, leading to less degradation in capacity when outdated channel state information is available.**

I. Introduction

Over the past few years, multiple-input multiple-output (MIMO) channel measurements have been made in different environments, for example, see the many results reported in [1]. It is clear that few real environments meet the idealised conditions suggested by models such as the isotropic scattering models of Clarke and Aulin [2, Ch. 2]. Rather, measurements such as those described in [3] show that the spatial characteristics are highly dependent on the local environment; this is reflected in the improved channel models in use currently, such as that proposed in [4].

Gains in spectral efficiency obtained using multiple antenna elements result from the spatial diversity of directional multipath components. Both specular reflection and scattering contribute directional components to the received signal and hence impact the spatial diversity. The relative contributions of these two mechanisms depend on the signal wavelength and the size of the interacting objects in the surrounding environment:specular reflection results from interactions with objects that are large relative to the signal wavelength, and scattering occurs from objects that are small relative to the wavelength [5].

Most of the measurement campaigns reported are targeted at understanding the characteristics applicable to space-time systems at carrier frequencies in the region of 1.8 GHz, 2.4 GHz or 5 GHz, which support commercial systems based on standards such as WiFi and WiMAX. It would be interesting to know what the impact of carrier frequency is on the potential for MIMO to provide high spectral efficiencies; in particular, for users who have allocations in the low UHF bands, whether the characteristics of urban vehicular MIMO channels obtained using measurements at higher frequencies can be translated to these bands.

The objective of the work presented herein was to investigate the characteristics of the vehicular urban MIMO channel at different UHF frequencies. This was achieved using measurements obtained in a microcell-type configuration in an urban environment, and analysed to investigate the spatial and temporal characteristics.

II. Measurements

The MIMO sounder developed at the Communications Research Centre was used to obtain channel measurements at three frequencies on routes in downtown Ottawa, Canada, using $N_t = 8$ and $N_r = 8$ antenna elements at the transmitter and receiver, respectively. For details on the sounder, see [6].

The carrier frequencies used were 2 GHz, 915 MHz and 370 MHz, and the bandwidths were 25 MHz, 10 MHz and 10 MHz, respectively. The 915 MHz measurement was made in the ISM band, and there was interference in many locations that degraded the capability of the measurement system to estimate the channel impulse responses. The received signals were sampled simultaneously at 50 Msamp/s (2 GHz) and 20 Msamp/s (915 MHz and 370 MHz), and the $N_r \cdot N_t$ channel impulse responses were obtained at a rate of 500 Hz.

The transmitter arrays were mounted on the roof of a trailer, at approximately 2.5 m above street level. The trailer was parked on the side of Lyon St. which has one-way traffic. The receiver arrays were mounted on the roof of a van, at about 2 m above street level, which was driven around an area of approximately two blocks radius. Due to the roof surface areas of the trailer and van, the transmitter and receiver arrays were limited in their overall dimensions. In particular, the 370 MHz elements were split into two uniform linear arrays at both terminals, with separations of approximately one-half wavelength. At the transmitter, the two subarrays were separated by two wavelengths, while on the van roof, the separation was 1.5 wavelengths. At the two higher frequencies, the elements were arranged in a single linear array at each terminal, with spacings of approximately one-half wavelength at 915 MHz and 2 GHz. The configuration of the arrays is illustrated in Fig. 1.

Because the antenna arrays at the transmitter and receiver are mounted above the height of most vehicular traffic, the dominant multipath components are received after interaction with the fixed infrastructure, in particular, buildings. This has been seen in previous work with the CRC MIMO sounder, in which the impact of traffic density on the channel characteristics was analysed and found to be relatively insignificant. Nonetheless, the measurements on each street were obtained

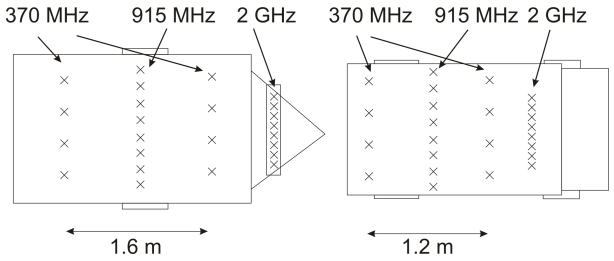

Fig. 1. Array configurations at the transmitter (trailer, static) and receiver (van, mobile).

for all three frequencies within one hour of each other, during a low traffic interval, 10:30 am–11:30 am on Kent St. and 1 pm–2 pm on Slater St. The measurement durations are approximately 25 s on Kent St. and 30 s on Slater St. (see Fig. 2).

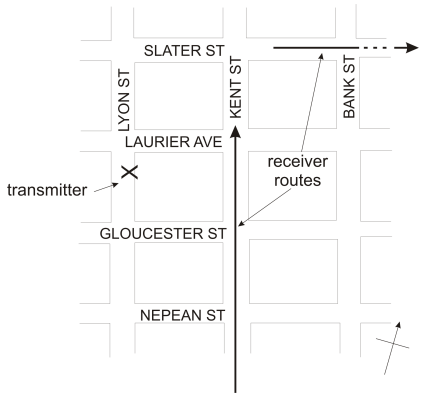

Fig. 2. Map of measurement routes in downtown Ottawa.

III. Channel Characteristics

The measured data were processed offline as described in [3] to obtain time-series of narrowband channel response matrices $\mathbf{H}(n)$, at intervals nT_s for $T_s = 2$ ms, for each frequency. The time-series have been analysed to assess their similarities and differences.

As the receiver position is not precisely aligned for the different measurements, it is not possible to compare very short segments of data. In fact, from previous work, e.g., [3], [7], it is known that the channel multipath structure is consistent only over intervals as short as 2 m. Either GPS resolution limits or the separation of antenna array structures on the van and trailer (Fig. 1) would therefore introduce sufficient uncertainty into the position that exact alignment of the measurements at different frequencies would be extremely challenging. To mitigate this uncertainty, in the following, characteristics will be compared over intervals of 2.5 s, where each such interval is selected to comprise a reasonably consistent scattering environment where the characteristics are broadly similar. As intervals of this length are not wide-sense stationary [3], the characteristics cannot be averaged. The distributions of particular metrics will therefore be compared to ascertain trends of characteristics.

A. Capacity

A preliminary assessment of the channel characteristics can be gained by examining the theoretical channel capacity for each MIMO channel. To this end, each time-series was normalised over its full length such that $\mathcal{E}\left\{\|\mathbf{H}(n)\|_F^2\right\} = N_r \cdot N_t$. The capacity was computed assuming no channel state information (CSI) is available at the transmitter, i.e.,

$$C(n) = \sum_i \log_2\left(1 + \frac{P\lambda_i(n)}{N_t\omega_n^2}\right) \quad (1)$$

where P is the total transmit power, divided equally among the N_t transmit elements, ω_n^2 is the variance of the AWGN, and $\lambda_i(n)$ is the ith eigenvalue of

$$\mathbf{R}(n) = \mathbf{H}(n)\mathbf{H}^H(n). \quad (2)$$

The capacity at a nominal SNR of 30 dB is shown in Fig. 3 for each of the three frequencies on Kent St. Note that, due to interference in the ISM band, the estimated channel responses at 915 MHz were of reduced quality, particularly in the first 10 s. The general capacity trends, resulting from the local scattering environment, are quite similar, for example, there is a clear increase in capacity as the mobile receiver crosses Laurier Ave. in the neighbourhood of 20 s, and another, smaller increase near 8 s at the intersection with Gloucester St.

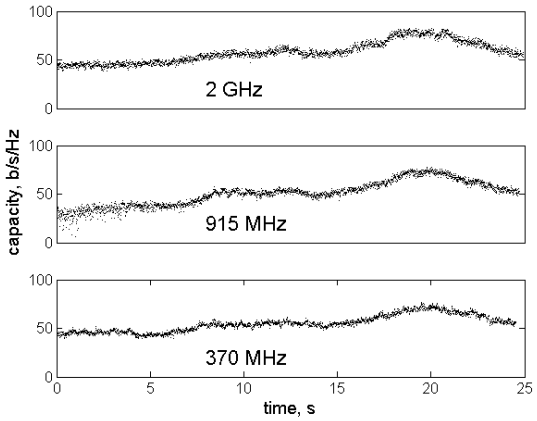

Fig. 3. Estimated capacity at 30 dB on Kent St.

On closer examination of shorter segments, it is seen that there are small-scale differences, in particular the estimated capacity decreases with frequency, in general; this is shown in Sec. III-B to be a result of lower spatial diversity.

From Fig. 3, two sub-series of the Kent St. measurement are selected for more detailed investigation: the first, 12.5-15 s, is within the block before the intersection with Laurier Ave., and 18.5-21 s is in and around that intersection. This intersection is of particular significance, because of the proximity of the transmitter to Laurier Ave., see Fig. 2. One segment from Slater St. is also selected, around the intersection with Bank St., i.e., 12.5-15 s.

B. Spatial diversity

For a series of $N_t \times N_r$ channel response matrices $\mathbf{H}(n)$, the full autocorrelation matrix

$$\mathbf{R}_{\mathbf{H}}(k) = \mathcal{E}\left\{vec\{\mathbf{H}(n)\}vec\{\mathbf{H}(n+k)\}^H\right\} \quad (3)$$

fully describes the spatio-temporal characteristics. In particular, the eigenvalues can be used to determine the degree of spatio-temporal diversity [1, Ch. 6]. However, computing $\mathbf{R}_{\mathbf{H}}(k)$ requires at least $N_r \cdot N_t$ independent samples. It was shown in [3] that the MIMO channel is rarely wide-sense stationary for intervals long enough to compute this matrix accurately. Therefore, here the spatial diversity is considered, defined at sample n as

$$d(n) = \frac{\mathrm{tr}\{\mathbf{R}(n)\}^2}{\|\mathbf{R}(n)\|^2} = \frac{\left(\sum_{i=1}^{N_r}\lambda_i\right)^2}{\sum_{i=1}^{N_r}\lambda_i^2} \quad (4)$$

where λ_i, $i = 1, \ldots, N_r$ are the eigenvalues of $\mathbf{R}(n)$, given by (2).

Histograms of the spatial diversity computed for each sample in the three data sub-series are shown in Figs. 4–6. The spatial diversity is lowest for all frequencies on Kent St. at the intersection with Laurier Ave., where there is a strong signal component from the west side of the vehicle, leading to increased spatial correlation and hence lower diversity. Note also that this corresponds to the region of greatest capacity in Fig. 3; this capacity is a result of the total received signal power, not spatial diversity. This effect is not observed in the measurement from Slater St. because there is no strong peripheral path along Bank St.

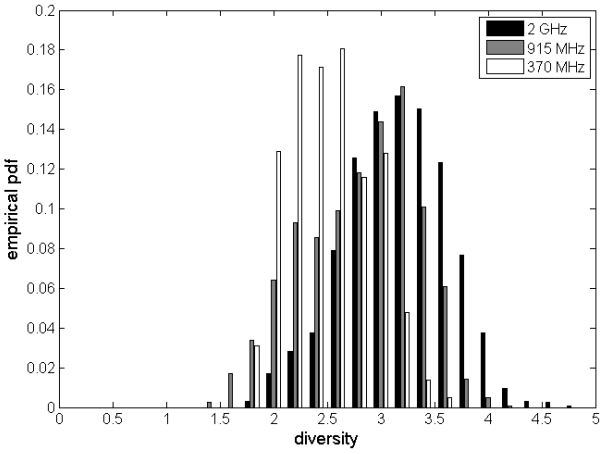

Fig. 4. Histogram of diversity observed on Kent St. from 12.5–15 s.

In general, the diversity increases with increasing frequency, although at the intersection on Kent St. (Fig. 5) the lowest diversity is measured for 915 MHz. The reason for this is not clear. In general, this variation of diversity with frequency is attributed to the increased scattering at lower frequencies, as more objects in the environment are small relative to the wavelength; objects that provide scattered or specular multipath contributions at higher frequencies become relatively too small

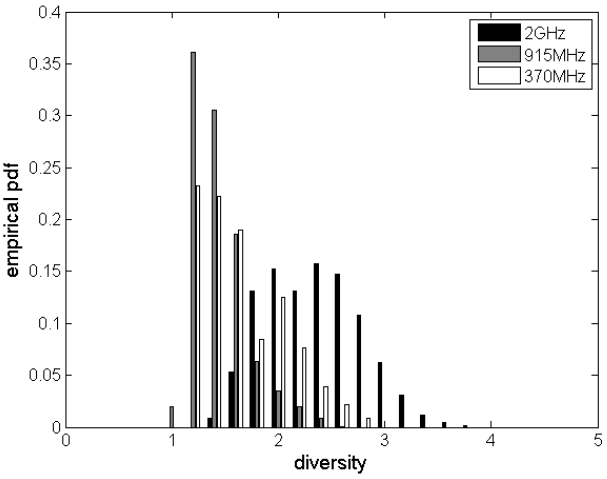

Fig. 5. Histogram of diversity observed on Kent St. from 18.5–21 s.

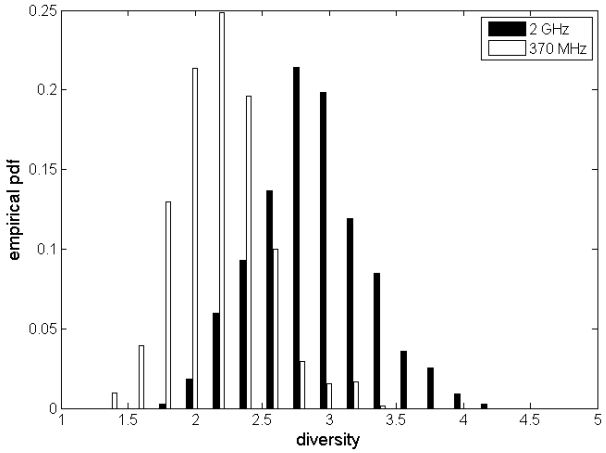

Fig. 6. Histogram of diversity observed on Slater St. from 12.5–15 s.

to contribute significantly as the wavelength increases. Therefore, the energy received through the scattering mechanism is reduced, leaving a smaller number of dominant specular components which leads to increased spatial correlation and lower diversity. This is supported by the higher variance in diversity observed at 2 GHz relative to the lower frequencies.

C. Capacity degradation

One measure of the time-varying characteristics of the MIMO channel is the degradation in capacity resulting from using an outdated channel response matrix. If the most recent channel response matrix available at the transmitter and receiver at time $(n+k)T_s$ is $\mathbf{H}(n)$, then the capacity was computed in [8] as

$$C_R(n,k) = \sum_i \log_2\left(1 + \frac{p_i\sigma_i^2(n)}{q_i}\right) \quad (5)$$

$$q_i = (\mathbf{M}\mathbf{P}\mathbf{M}^H)_{ii} + \omega_n^2 \quad (6)$$

$$\mathbf{M} = \mathbf{U}^H(n)\mathbf{H}(n+k)\mathbf{V}(n) - \mathbf{\Phi}(n,k)\mathbf{\Sigma}(n) \quad (7)$$

where the singular value decomposition (SVD) of the channel matrix is $\mathbf{H}(n) = \mathbf{U}(n)\mathbf{\Sigma}(n)\mathbf{V}^H(n)$, and the diagonal elements of $\mathbf{\Sigma}(n)$ are the singular values $\sigma_i(n)$, $i = 1, \ldots, \min(N_r, N_t)$. The signal covariance matrix $\mathbf{P} = diag(p_1, \ldots, p_{N_t})$, where p_i is the power allocated to the ith data stream using the waterfilling solution at time n, and $\text{tr}(\mathbf{P}) = P$. The diagonal matrix $\mathbf{\Phi}$ has non-zero elements $|\Phi_{ii}| = 1$, and the phases of these elements are selected such that the diagonal elements of $\mathbf{M}$ are real.

The capacity degradation, $C_R(n,k)$ has been computed for the sub-series of interest on both Kent and Slater Streets at $P/N_r\omega_n^2 = 30$ dB. As noted above, the time-series are not WSS over these intervals, therefore the computed values of $C_R(n,k)$ cannot be meaningfully averaged over n. The characteristics of the difference frequencies are compared by determining the range of delays at which $C_R(n,k)$ drops below 50% of $C_R(n,0)$. Figs. 7–8 show histograms of this delay over the Kent St. sub-series. As for the spatial diversity, the capacity degradation observed on Slater St. in the range 12.5-15 s is similar to those on Kent St. in the 12.5-15 s interval.

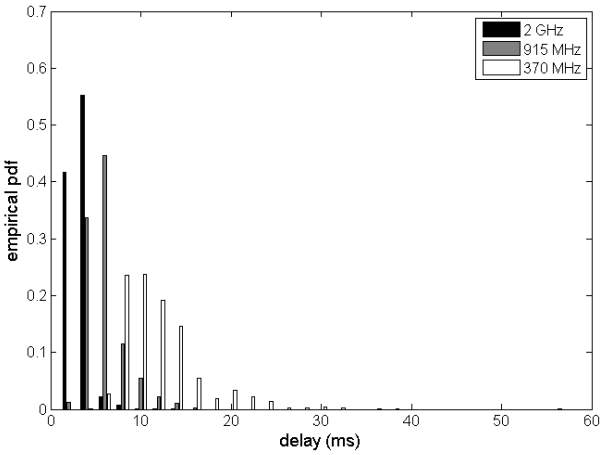

Fig. 7. Histogram of delays such that $C_R(n,k)/C_R(n,0) = 0.5$ on Kent St. from 12.5–15 s.

These figures show that the capacity varies more rapidly at higher frequencies. This is anticipated because the autocorrelation of the received signal is a function of the maximum Doppler frequency, f_m, e.g., for isotropic scattering the autocorrelation at delay τ is the well-known $J_0(2\pi f_m \tau)$ where $J_0(\cdot)$ is the zeroth-order Bessel function of the first kind. Thus, even for non-isotropic scattering, the autocorrelation decreases more slowly with τ at larger wavelengths.

D. Eigenstructure

The capacity degradation metric $C_R(n,k)$ combines the effect of the changes in the eigenvalues $\lambda_i(n)$ and eigenvectors $\mathbf{u}_i(n)$ of $\mathbf{R}(n)$ given in (2). These eigen-characteristics are important for adaptive MIMO signalling schemes based on the eigenvalues, such as the orthonormal diversity-multiplexing precodes in [9], or on the eigenvectors, such as [10]. To

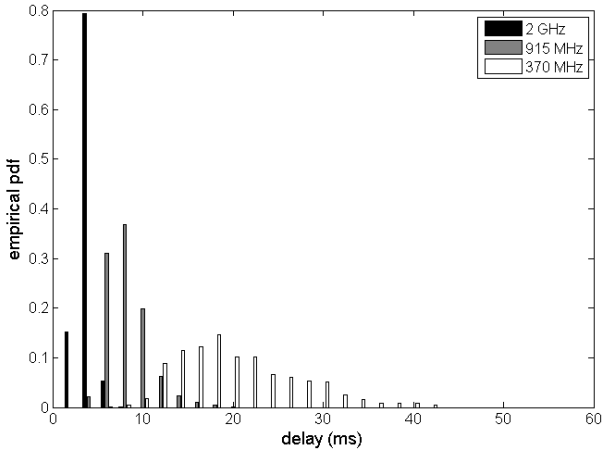

Fig. 8. Histogram of delays such that $C_R(n,k)/C_R(n,0) = 0.5$ on Kent St. from 18.5–21 s.

illustrate the rate of change in these structural features, the eigenvalue correlation

$$\phi_{\lambda_i\lambda_i}(k) = \frac{1}{N}\sum_{n=1}^{N}(\lambda_i(n) - \bar{\lambda}_i)(\lambda_i(n+k) - \bar{\lambda}_i) \qquad (8)$$

where $\bar{\lambda}_i$ is the mean value of $\lambda_i(n)$ over the block, and the eigenvector correlation

$$\phi_{\mathbf{u}_i\mathbf{u}_i}(k) = \frac{1}{N}\sum_{n=1}^{N}\mathbf{u}_i^H(n)\mathbf{u}_i(n+k) \qquad (9)$$

were computed. The sub-series were broken into overlapping blocks of length $N = 80$ samples, or 160 ms; this length was determined to be appropriately assumed as quasi-stationary in [3] for the same propagation environment. As before, these autocorrelation functions cannot be averaged over different blocks; the eigenvalue correlation is compared through the delay d_{λ_i} at which $\phi_{\lambda_i\lambda_i}(k)$ drops to 50% of its value at $k = 0$. The eigenvector autocorrelation $\phi_{\mathbf{u}_i\mathbf{u}_i}(k)$ has the general form of a damped oscillation around a decreasing trend: in this case, the distributions of delays $m_{\mathbf{u}_1}$ to the first minimum are compared.

The histogram of delays $m_{\mathbf{u}_1}$, for the dominant eigenvector $\mathbf{u}_1(n)$, on Kent St. in the time interval 12.5–15 s is shown in Fig. 9. At 2 GHz, the first minimum is predominantly around 8-10 ms, compared to approximately 14 ms at 915 MHz and 32 ms at 370 MHz. The spread also increases as the frequency decreases.

Each block of length 160 ms is assumed quasi-stationary, which means that the multipath components arrive with the same power from the same angles of arrival over the whole length. These angles are determined by the surrounding infrastructure, and are therefore more-or-less independent of frequency. However, the rotation of the eigenvectors is faster at higher frequencies because the rate of change of the phase differences among the multipath components as the receiver moves is dependent on the Doppler shift. As seen in Fig. 10,

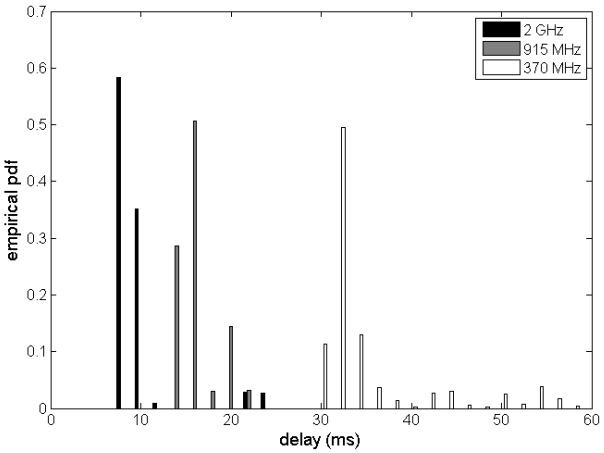

Fig. 9. Histogram of delays $m_{\mathbf{u}_1}$ to the first minimum in $\phi_{\mathbf{u}_i\mathbf{u}_i}(k)$ on Kent St. from 12.5–15 s.

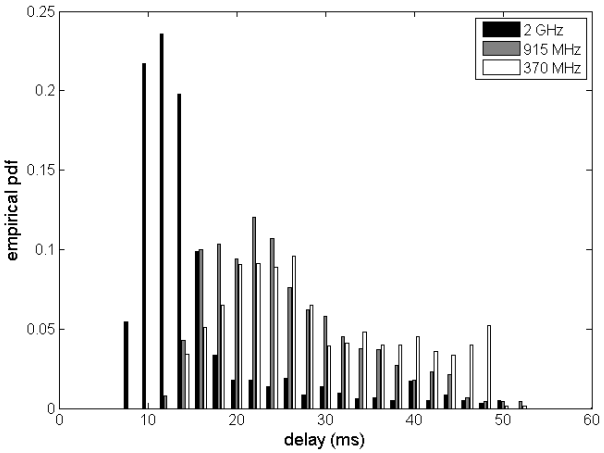

Fig. 11. Histogram of delays d_{λ_1} such that $\phi_{\lambda_1\lambda_1}(d_{\lambda_1})/\phi_{\lambda_1\lambda_1}(0) = 0.5$ on Kent St. from 18.5–21 s.

the eigenvalues vary faster because they also directly incorporate the impact of the transmitter surroundings, but again the dependence on frequency is clear.

Note that the eigenvectors are more stable around the intersection with Laurier Ave. – the first minima are observed later for the interval starting at 18.5 s, around 16 ms (2 GHz), 30 ms (915 MHz) and in excess of 50 ms (370 ms), but are also much shallower compared to the previous interval. In this range, there is a strong specular component from the direction of the transmitter: this stabilises the eigenstructure for all frequencies. In this case, the variation in capacity (Fig. 8) is due primarily to the change in eigenvalues, as seen in Fig. 11, which shows d_{λ_1}, for the strongest eigenvalue, λ_1, over this interval. The variation is slower than for the interval in the urban canyon, but again it increases as the frequency decreases.

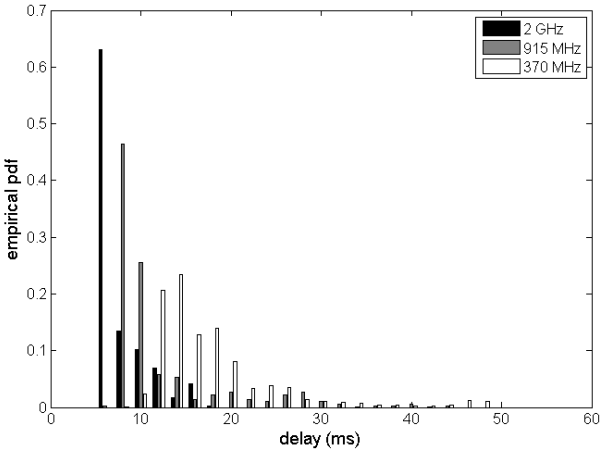

Fig. 10. Histogram of delays d_{λ_1} such that $\phi_{\lambda_1\lambda_1}(d_{\lambda_1})/\phi_{\lambda_1\lambda_1}(0) = 0.5$ on Kent St. from 12.5–15 s.

IV. Conclusions

Measurements were obtained at three frequencies spanning the UHF band in urban Ottawa, and have been analysed to determine their characteristics. The spatial diversity is lower at lower frequencies, this is attributed to an increase in scattering at larger wavelengths which reduces the number of signal components received. This lower spatial diversity leads to a reduction in capacity of up to 10% from 2 GHz to 370 MHz. However, at lower frequencies, the structural composition of the MIMO channel varies more slowly. This suggests that the loss in diversity might be compensated by a reduced overhead requirement for pilot signals and feedback for adaptation.

Acknowledgements

This work was supported by Defence Research and Development Canada.

References

[1] L. M. Correia, Ed., *Mobile Broadband Multimedia Networks*. Academic Press, 2006.

[2] G. L. Stüber, *Principles of Mobile Communication*. Kluwer Academic Publishers, 2001.

[3] T. J. Willink, "Wide-sense stationarity of mobile MIMO radio channels," *IEEE Trans. Veh. Technol.*, vol. 57, no. 2, pp. 704–714, Mar. 2008.

[4] W. Weichselberger, M. Herdin, H. Özcelik, and E. Bonek, "A stochastic MIMO channel model with joint correlation of both link ends," *IEEE Trans. Wireless Commun.*, vol. 5, no. 1, pp. 90–1001, Jan. 2006.

[5] R. Vaughan and J. B. Andersen, *Channels, Propagation and Antennas for Mobile Communications*. IET, 2003.

[6] C. Squires, T. Willink, and B. Gagnon, "A flexible platform for MIMO channel characterization and system evaluation," in *WIRELESS 2003 - Proc. 15th Conf. on Wireless Commun.*, Calgary, Canada, July 2003.

[7] R. J. C. Bultitude, "Methods for estimating consistency intervals, and the detection of changes on mobile radio channels," in *Proc. XXIX URSI General Assembly*, Chicago, IL, USA, Aug. 2008.

[8] J. W. Wallace and M. A. Jensen, "Time-varying mimo channels: Measurement, analysis, and modeling," *IEEE Trans. Antennas Propagat.*, vol. 54, no. 11, pp. 3265–3273, Nov. 2006.

[9] G. W. K. Colman and T. J. Willink, "Orthonormal diversity-multiplexing precoding in MIMO systems at finite SNR," *IEEE Commun. Lett.*, vol. 11, no. 8, pp. 650–652, Aug. 2007.

[10] S. Zhou and G. B. Giannakis, "How accurate channel prediction needs to be for transmit-beamforming with adaptive modulation over Rayleigh MIMO channels?" *IEEE Trans. Wireless Commun.*, vol. 3, no. 4, pp. 1285–1294, July 2004.